- consistent use of Nomenclature (eg. cell line ref.)
- use Abbreviations!
- Language / Expression: check Sentences
- Don't use Appendix A for details.
- Experiments: Synched vs. non-synched. Das muss hier rein. Define name!

OR: microSlit vs. microtrack

OR: PEG-DA vs. PEGDA

Chapter 2

Data and Methods

This chapter considers two aspects of the project: the experiment setting and the data analysis pipeline. In the first half of the chapter, the cell environment is brought forth. The highlight of this experiment, the microfluidics setup for cell containment, is elucidated in this part. Some biomedical and biochemistry aspects of the experiment are also mentioned. This includes the drugs and the auxiliary chemicals of interest used in the experiment, and the cell lines probed for the experiment. Later on, the hypothesis underlying the experiment is presented.

The second part deals mostly with the quantitative methods and algorithms used to process data into meaningful observations. The part is opened with definitions used in the methods section. Afterwards, each method developed/used in the pipeline is brought forward. For each method, the rationale explaining the reason of using the method is also accompanied in the subsection.

2.1 Experimental Setting and Data

2.1.1 Cell Culture

For easier analysis and comparison of experiment resutlts vis-a-vis related experiments, a model cell line is used. In this project, a strain of acute monocytic leukimia (AML) in used: the AML-M5a MOLM-13 cell line. The line used in this experiment derived itself from the cell line initially described by Matsuo *et al.* in 1997 [4]. In the paper, the authors developed the line from the peripheral blood of a relapse patient with acute monocytic leukemia (AML) of subtype FAB M5a, which is characterized by predominantly monoblastic leukemia cells in patient sample [5]. Various studies on the cell lines have made it an ideal candidate for studying *in vitro* study of monocytic differentiation, leukemogenesis and treatment dynamics [4, 6].

For the experiment, the acute monocytic leukemia (AML-M5a) MOLM-13 cell line was cultured in Gibco® RPMI 1640 GlutaMAX medium, produced by Life Technologies [7]. The medium is a popular option in human cell biology for experiment and biological synthesis based on human cells and their derivatives [8, 9]. It is pre-supplemented with a stable form of L-glutamine to prevent ammonia buildup, a common and serious problem in cell culture due to its cell toxicity[10]. The medium is further supplemented with Gibco® Fetal Bovine Serum (FBS), also offered by Life Technologies [11], as supplement for the AML-M5a MOLM-13 cell culture.

Some other cell lines were also appraised as potential cell line of interest in this experiment. One of them is Jurkat Cell, a model cell commonly used to study T Cell Leukimia, T cell signalling mechanism and the expression of various HIV-related chemokines [12]. The cell line was a considered since it is well-studied [13, 14]. This is especially true if we consider apoptotic mechanism of the cell line, a problem this project and other related projects by our and partner labs are trying to investigate. There are several seminal publications about the dynamics of apoptotic mechanism of Jurkat cells we could well compare our results to [15]. Samali *et al* [16] even studies the dynamics of caspase expression in Jurkat cells, a topic dealt a lot in this project as the chapters progress (see for example Section TODO fill on cell death signal) while Kasai *et al* considers the aspect of spindle checkpoint in the context of apopototic cell death [17]. However, we figured out early on that the cell motility of the Jurkat cell line was increased dramatically (a phenomenon observed by others before us [18]) upon the introduction of chemotherapeutic treatment – the increase dramatic enough that the cells managed to escape the microslit it initially landed in.

2.1.2 Microfluidics ~~environment~~

The ~~general~~ term ~~of~~ 'microfluidics' concerns the wide application of micro-sized devices, which hold and control the state of liquid. ~~This~~ includes cell culture medium. There are two categories of microfluidics: active and passive devises. The separation is based on the device's ability to actively manipulate the flow and control of devices. Active devices ~~such~~ as micro-valves ~~can~~ perform sophisticated chemical processes [19]. This goes as far as reactions at individual cell level [20]. While passive devices, such as micro-arrays, provide a rapid parallel observation platform.

Active microfluidic methods for analysis and manipulation of biological cells have been done in various way and form. In 2003, Wheeler *et al* developed a novel microfluidic device from poly-dimethylsioxane using multilayer soft lithography technology for the analysis of single cells [21]. The microfluidic setup facilitates the passive and gentle separation of a single cell from the bulk cell suspension. This in turn enables the precise delivery of reagents as little as one nanoliter to the cell. In other use cases, the optical-based microfluidic methods have been used to sort cell with very high accuracy [22]. This family of methods utilizes the fact that different dielectric particles respond differently to an applied light field [23]. Combined with the miniscule spatial setting, the methods are compatible for single-cell resolution analysis. For example, optical-based microfluidic methods have been used to sort cells with very high accuracy [22, 24, 25].

~~As a method~~, passive mocrofluidic methods are mostly used to provide specialized environment in cell-size resoultion. For example, microfluidic ~~settings~~ have been used to keep spatio-temporal identity of single cell for the analysis of the underlying biological dynamics of the isolated cells [26, 27], which form the methods the design and synthesis of our microtrench environment are based on.

In our cases, the microfluidic settings trace back to the works of our partner lab at Biophysics Department at Ludwig-Maximillians-Universität München in 2013 [28] and 2015 [27, 29].

In order to track in a label-free manner ~~non-adherent cells~~ over several generations, ~~we~~ designed and fabricated micro-trenches ($30 \times 120\,\mu m$) out of PEG-DA (Polyethylene(glycol) Diacrylate), which can accommodate four to six cells. The ~~proposed~~ platform

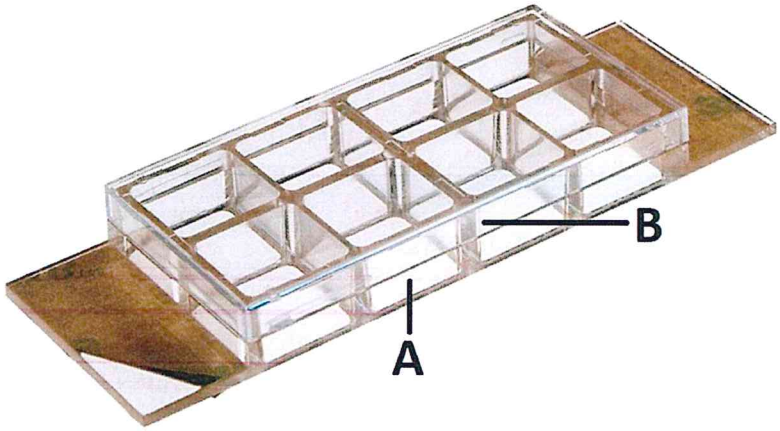

Figure 2.1: ibidi® sticky-Slide 8 Well. The base SU-8 wafer is located in each of the containment box (**A**). The SU-8 wafer is then fabricated in the surface of each containment box using nano photolitographic printing. The microfluidics system is then poured and stamped on top the wafer (see Appendix A for detailed manufacturing process). Note that each containment box is upside-open. The cap (**B**) is used to prevent the ingress of foreign materials into the medium. *Image taken and modified from ibidi GmbH's website.*

2.3.3 Shift Correction

Now, consider a case in which images are shifted in a time-lapsed movie. TODO: explain mechanism. No rotation of camera is assumed, hence there are only two degree of freedoms (vertical and horizontal). Thus, a shift can be defined as a vector movement $\vec{v}$ of all points $x_{i,j} \in M_{t_i}$ in the time-lapse from time t_i to t_{i+1}. Given two degrees of freedom and discreteness of the problem due to pixel representation, the task is reduced to finding difference in x- and y-axis (δ_x and δ_y), so that the difference of transformed pixels at t_i and t_{i+1} are minimized, i.e.:

$$argmin_{\delta_x,\delta_y}\{d(M_{t_i}, M_{t_{i+1}}^{\delta_x,\delta_y} + (\delta_x, \delta_y)^T)\}$$

Where $M_{t_{i+1}}^{\delta_x,\delta_y}$ is the entries of matrix $M_{t_{i+1}}$ after applying the shift $\vec{v} := (\delta_x, \delta_y)^T$, i.e.

$$M_{t_{i+1},x,y}^{\delta_x,\delta_y} = M_{t_{i+1},x-\delta_x,y-\delta_y}$$

For the distance function d, the in all channels absolute difference function is used, which is defined as:

$$d(M_i, M_j) = \sum_{c \in \{R,B,G\}} \sum_x \sum_y |M_{i,c,x,y} - M_{j,c,x,y}|$$

facilitated cell tracking, leading to the observation of hundreds of families of cells, derived from one single mother at each case. This enabled us firstly to study the distribution of division times among single cells and also to correlate the division times between sister cells, which are genetically identical. Secondly, the array of micro-trenches enabled the study of the response dynamics of single-cells to doxorubicin, a widely used chemotherapeutic drug, and the comparison of the response to this agent between a chemically synchronized and a non-synchronized population. The detailed methods and protocols for the fabrication of the microfluidics system used in the experiment could be found in Appendix A. The design of the microslit and the schematic representative of cell tracking are seen in Figure 2.2.

The experiment setting looks as follows:

The microtrenches:

The smallest structure of the setting, measuring about 120 microns by 30 microns. The base of the slit is made of Polyethylene (glycol) Diacrylate (PEGDA), an inert substance commonly found as construction material in microfluidics system [27]. Each tretment contains about 2400 microtrenches (See ~~Results~~ section) contained in one containment box.

The containment system:

The trench could contain up to 8 cells. The macro-container chosen for containing the wafers holding the microtrenches is ibidi® sticky-Slide 8 Well (see Figure 2.1). In the project, each cell treatment is isolated in one containment box. This ensure the separations of different chemicals used in each treatment.

2.2 Definitions

Mathematical definitions used in the thesis

2.3 Methods

2.3.1 Laplacian of Gaussian (LoG) Cell Recognition

2.3.2 Image Encoding

Consider following picture:

There are numerous encodings that could be used to internally represent this picture. Many such encodings derived from the so-called Red-Green-Blue (RGB) encodings [30]. RGB encoding represents the pixel as a combination of red, green and blue color. This encoding is able to represent various spectra of human visible color and useful enough for most use cases [30, 31]. To give representation on how the encoding works, the RGB encoding of some part of Figure ?? is shown in Figure 2.5. For an image of size $m \times n$ pixels, the RGB encoding is thus a 3-dimensional matrix of dimension $m \times n \times 3$. For time-lapsed images accordingly, the RGB encoding of a video of length T is a 5-dimensional matrix of shape $T \times m \times n \times 3$. TODO: put graphical explanation of data here.

Don't show images from old setup!

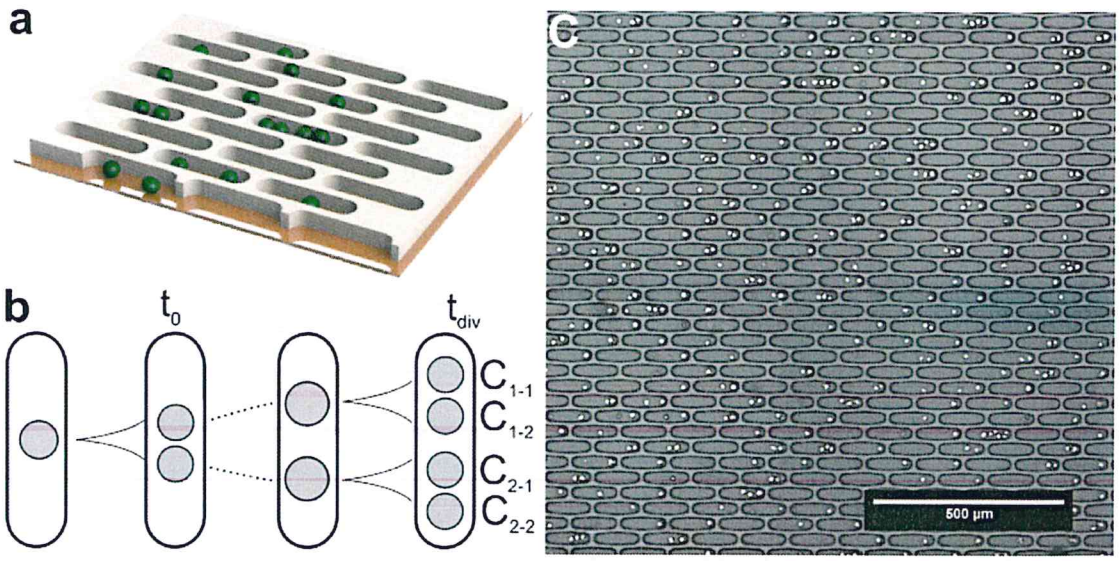

Figure 2.2: The structure of microslits: **(A)** 3D model of microslit on surface with cells inside. **(B)** The schematic representation of a time-lapse in a trench. First, a singly-placed cell is tracked in a slit. At time t_0, the cell divides into two daughter cells. The two cells will be kept tracked until at one point each of the daughter cells will divide at the same time at time t_{div}. Note the simplification of the sample. First, not every cell is singly-placed inside a trench. Indeed, not every trench is occupied by cells. Second, not every cell divides. Third, not every cell line observed has three generations in it. And finally, not every children's division times are at the same time. Indeed, this special case almost never happens in real life. **(C)** The sample view into the environment with cells occupying some slits. Here, the microslits have dimension of 120 μm long and 30 μm wide. Note also the pointish characteristic of the cells taken in out-of-focus fashion. This improves the performance of the tracking algorithms. *Figure taken from (Sekhavati, 2015) [29].*

is this your text?

Since some pixels are lost from the field of view during a shift, only a subset of subsequent pictures is used to determine the shift, preferably those around the center point. This will allow the largest search space possible, since the distance to all four margins of the picture is maximized at the center point. The search for the optimal (δ_x, δ_y) pair is implemented as a grid search along the x- and y-axis. An example of the search grid is shown in Figure 2.6.

Since the time-lapsed data consists mainly of grayscale image, the RGB encoding could be the directly transformed to grayscale encoding. Using the transformed method also speeds up the calculation process since the distance function only computes the difference of grayscale channel's values:

$$d(M, N) = \sum_x \sum_y |M^{gray}_{c,x,y} - N^{gray}_{x,y}|$$

Due to lost pixels around the margin of before and after pictures, only the overlapping part of both slides are included after the correction. Thus, for an inferred shift of (δ_x, δ_y),

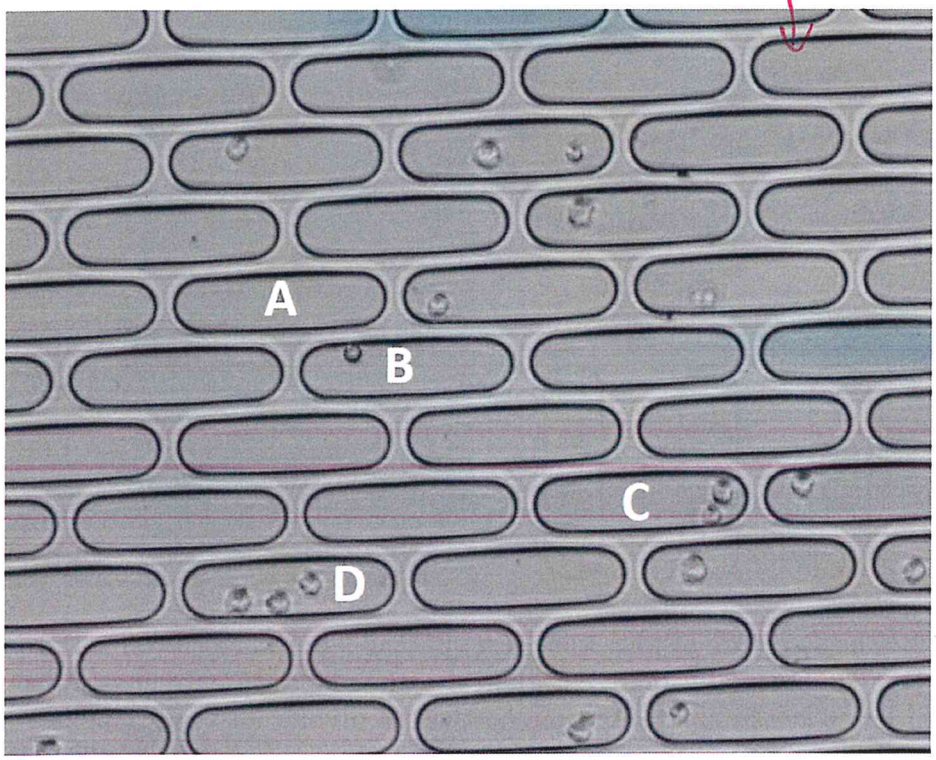

Figure 2.3: ~~The typical view of microslit setting~~. Some slits contai no cell at all (**A**). Several slits contain exactly one cell (**B**). A few ~~more~~ slits contain two cells (**C**) while in rare cases ~~the~~ slit ~~could~~ contain more than two cells (**D**).

the new dimension of the pictures is then $(m - \delta_x) \times (n - \delta_y)$. This change would then propagation to the other time-lapse images to maintain consistency of the images.

Ideally, the shift correction should be done for each position to reduce the track dropout rate caused by image shifts. This is however computationally very expensive and, as seen in Figure 2.7, not really necessary since the biggest shift indeed only happens right before and after the treatment, as it was expected during the experiment setting. As seen in Chapter XX (TODO: quote), the tracking allows certain amount of tolerance. In this regard, the other frame shifts are way within the tolerance of our tracking algorithm. As shown in Figure YY (TODO: add droput rate), the dropouts caused by frame shifts in the other time points are basically noisy dropout caused by random noise in time-lapse movie being tracked as cells [32].

The algorithm for shift inference is available in Appendix B.

2.3.4 Cell death signals

Measuring cell death is a crucial part of the experiment, as the reliable determination of it is the basis of most analysis in this thesis. There are several way to measure cell deaths with varying complexity and accuracy. Each method contains certain assumptions of cell death.

For example, determining cell death by cell movement assumes death of a cell if no